Short-time Brownian motion in colloidal suspensions: Experiment and simulation

P. N. Segrè, O. P. Behrend, and P. N. Pusey
Department of Physics and Astronomy, The University of Edinburgh, Mayfield Road, Edinburgh, EH9 3JZ, United Kingdom
(Received 6 June 1995)

We used dynamic light scattering (DLS) and computer simulations based on the fluctuating lattice Boltzmann equation (LBE) method to study the short-time Brownian dynamics of colloidal particles that interact like hard spheres. The dynamics are characterized by a Q-vector-dependent diffusion coefficient $D_S(Q)$. Using DLS, we have mesaured $D_S(Q)$ in the vicinity of the main (first) peak in the structure factor $S(Q)$ for samples of poly-methylmethacrylate particles at volume fractions ϕ ranging from dilute up to the disorder-order transition (i.e., crystallization at $\phi=0.494$). In addition we have determined the short-time self-diffusion (D_S^S) and collective-diffusion D_S^C coefficients. We have extracted the same quantities from simulations of equilibrium configurations of hard spheres using a fluctuating lattice Boltzmann equation method for the fluid phase coupled to Newtonian mechanics for the colloidal particles. For all samples studied, close quantitative agreement is found between the results of the DLS experiments and the LBE simulations.

PACS number(s): 05.40.+j, 47.15.Pn, 82.70.Dd, 82.70.Kj

I. INTRODUCTION

The dynamics of colloidal suspensions have been the subject of continuing research over the past two decades (see references in [1]). The motion of Brownian particles suspended in a liquid is characterized by three distinct time regimes. For long times $\tau \gg \tau_R$, their motion is diffusive, resulting from interactions with the surrounding fluid and random encounters with other particles. This is the Brownian *long-time* regime. The time $\tau_R = R^2/D_0$, needed for a particle in a dilute suspension to diffuse over a distance comparable to its radius, is an estimate of the time scale on which direct interactions between the particles become important. Here R is the radius of a particle and D_0 is the diffusion coefficient at infinite dilution given by the Stokes-Einstein relation $D_0 = k_B T/6\pi\eta_0 R$; k_B is the Boltzmann constant, T the temperature, and η_0 the shear viscosity of the suspending fluid. At shorter times $\tau_B \ll \tau \ll \tau_R$, the motion is also diffusive, albeit at a faster rate, reflecting the fact that the particles have not yet been slowed down by direct interactions with neighboring particles. This is the Brownian *short-time* regime and the only interparticle interactions are the hydrodynamic interactions transmitted by the fluid. The Brownian relaxation time τ_B characterizes the time taken to decouple the dynamics of the colloidal particles from the dynamics of the fluid and is given by $\tau_B = m/6\pi\eta_0 R$, where m is the mass of a suspended particle. There is a clear separation between the two time scales τ_R and τ_B [1], allowing for the definition of distinct short- and long-time dynamics. On even shorter time scales $\tau \lesssim \tau_B$, the motion of the particles evolves from ballistic to diffusive as the velocities imparted to the particles by the collisions with fluid molecules are viscously damped. This is the *pre-Brownian* time regime.

On the theoretical side, progress in the description of the dynamics has been hindered by the complexity of the hydrodynamic interactions between the suspended particles; these interactions are of many-body nature and long range [1]. The work of Beenakker and Mazur [2] is the most comprehensive study of the short-time dynamics to date. Their work is based on a partial resummation of the hydrodynamic interactions, evaluated via a renormalized density fluctuation expansion. For the long-time regime, theoretical investigations are scarce and we only cite here the works of Medina-Noyola [3] and Tokuyama and Oppenheim [4], which both have investigated the self-motion of the particles. Reference [4] also contains work on the short-time self-motion, although the physical content of this theory remains to be elucidated fully. In the pre-Brownian regime, the hydrodynamic interactions are developing from local forces at the particle-fluid interface, which then diffuse through the fluid [1]. The hydrodynamic interactions of a *single* Brownian particle with the surrounding fluid lead to the so-called long-time tails in the decay of the velocity autocorrelation function of the Brownian particle. Much theoretical work has been done on this effect [5]; no theoretical predictions are, however, available on the development of the interactions between *several* particles.

On the experimental side, dynamic light scattering (DLS) has been used for many years to study colloidal suspensions by measuring the decay in time of the density fluctuations [1,6]. DLS has access to time scales $\tau > \tau_B$ and is thus ideally suited to investigate the short- and long-time Brownian dynamics. The decay of the density fluctuations can be characterized by a time-dependent and wave-vector-dependent diffusion coefficient $D(Q,\tau)$ and extensive data on the self- ($Q \to \infty$) and collective ($Q \to 0$) motion on the short time scale exist (see references in [1]). Some data at intermediate wave vectors also exist [7], but are limited by experimental uncertainties, principally due to multiple scattering effects. DLS measurements of the long-time self-motion have been previously reported [8,9], but no measurements at intermedi-

ate wave vectors in this time regime are available. Investigations of the pre-Brownian regime are very difficult via conventional DLS and have only become practical with the advent of diffusive wave spectroscopy (DWS) [10,11].

On the computational side, results have, until recently, been limited to the time scales $\tau > \tau_B$. The reason for this is that in the conventional computational methods for simulating colloidal suspensions, such as Brownian dynamics [12] or the multipole method [13], the hydrodynamic interactions between particles are considered to act instantaneously and their time-dependent development is not simulated. Thus these methods are suited only to time scales where these interactions are fully established $\tau > \tau_B$. Another consequence of this time-scale separation is that the interactions are *global,* depending on the positions of *all* the particles simulated; thus the algorithms scale mostly as the cube of the number of particles, making them computationally extremely expensive. Results have been reported for the short-time self- and collective-diffusion coefficients [13] from simulations that take full account of the hydrodynamic interactions. At intermediate wave vectors, only calculations using Brownian dynamics coupled to an empirical two-particle hydrodynamic interaction have been reported [14]. The long-time regime is practically inaccessible for the conventional algorithms due to the intense computations necessary. Only for systems where the hydrodynamic interactions can be neglected have the self-motion [15] (hard spheres without hydrodynamic interactions) and the wave-vector-dependent dynamics [16] (charged spheres) been investigated; alternatively, the self-motion of hard-sphere systems with hydrodynamics based on empirical pairwise additive hydrodynamic forces [17] has also been studied.

Recently, a numerical method for the simulation of colloidal suspension has emerged. It is based on a fluctuating lattice Boltzmann equation (LBE) method for the fluid phase coupled to Newtonian mechanics for the suspended hard-sphere particles [18–20]. This technique has been shown to fully simulate the hydrodynamic interactions in concentrated suspensions [19,20]; moreover, it captures the time-dependent development of these interactions from purely *local* forces and is thus suited for the study of the dynamics on *all* time scales. The locality of the interactions has as a consequence that the algorithm scales linearly with the number of particles, although, if a steady-state solution is to be reached, some allowance must be made for the full establishment of the time-dependent flows. However, even taking this additional computational expense into account, the algorithm represents a considerable improvement over conventional methods. Over the past few years, this method has been used, together with DWS experiments, to investigate the pre-Brownian regime [18,21]. Very interesting scaling behavior of $D(Q,\tau)$ has been observed and the combined use of experiment and simulation has led to additional insight into the time-dependent development of hydrodynamic interactions.

The aim of the work reported here is to extend this combined experimental and computational study of the dynamics of colloidal suspensions to time scales $\tau > \tau_B$, using DLS (experiment) and LBE (computation) methods. In the present paper, we concentrate on the short-time dynamics $\tau_B \ll \tau \ll \tau_R$, while in a future paper [22], we plan to discuss the data over all times $\tau > \tau_B$, with a focus on the long-time Brownian regime $\tau \gg \tau_R$.

We present here measurements of the short-time diffusion coefficient $D_S(Q)$, defined as the limit $\lim_{\tau_B \ll \tau \ll \tau_R} D(Q,\tau)$, for particle volume fractions ϕ ranging from dilute up to the disorder-order transition at $\phi_f = 0.494$ and for a range of wave vectors in the vicinity of the main peak in the structure factor $S(Q)$. We are thus probing the dynamics on length scales comparable to the interparticle separation, where the structural effects are the strongest. Our results will be compared to the theory of Beenakker and Mazur [2]. We will also present results for short-time *self-diffusion* $D_S^S \equiv D_S(Q \to \infty)$ and compare them to the theory of Ref. [2] and a more recent theory of Tokuyama and Oppenheim [4], as well as results for the short-time collective diffusion $D_S^C \equiv D_S(Q \to 0)$.

Our experimental results are obtained by dynamic light scattering from suspensions of poly-methylmethacrylate (PMMA) particles. Circumstantial evidence suggests that these particles interact like hard spheres [1] and we will confirm this conjecture in the present work. We use the two-color dynamic light scattering (TCDLS) method [23], which eliminates the effects of multiple scattering in turbid samples. We thus believe our data to be more accurate than previous measurements of the Q-dependent diffusion coefficients [7], which, especially at low Q vectors where the effects of multiple scattering are strong, had quite large experimental errors. Moreover, we describe accurate methods to determine both the particle radii and the sample concentrations. Both of these quantities, especially the particle volume fraction ϕ, must be accurately determined before any meaningful comparison to theory and simulation can be made.

II. THEORY

The intermediate scattering function of a system of N particles is given by [6,24]

$$F(Q,\tau) = \frac{1}{N} \sum_{i,j} \langle \exp\{i\mathbf{Q}\cdot[\mathbf{r}_i(0) - \mathbf{r}_j(\tau)]\} \rangle \ . \tag{1}$$

Here the angular brackets $\langle\ \rangle$ denote an average over an ensemble of equilibrium distributions, $\mathbf{r}_i$ is the position of the center of mass of particle i, where $i,j = 1, \ldots, N$, and τ represents time. $F(Q,\tau)$ (which in isotropic samples depends on the magnitude Q of the scattering vector $\mathbf{Q}$ only) is the spatial Fourier transform of the particle number density autocorrelation function. The zero-time value of the scattering function gives the static structure factor $F(Q,0) = S(Q)$. The normalized scattering function $f(Q,\tau) = F(Q,\tau)/S(Q)$ is the quantity most easily measured by dynamic light scattering experiments. The decay of the density fluctuations, characterizing the dynamics of the system, can be expressed by considering the time derivative of $f(Q,\tau)$,

$$\frac{\partial f(Q,\tau)}{\partial \tau} = -Q^2 D(Q,\tau) f(Q,\tau) \ . \tag{2}$$

Here we have introduced the time- and wave-vector-dependent diffusion coefficient $D(Q,\tau)$, which depends on both structural and hydrodynamic effects. The particle dynamics are diffusive if $D(Q,\tau)$ is time independent and the decay of $f(Q,\tau)$ is exponential. This is the case in the Brownian short-time regime $\tau_B \ll \tau \ll \tau_R$ and the associated diffusion coefficient is $D_S(Q) \equiv \lim_{\tau_B \ll \tau \ll \tau_R} D(Q,\tau)$ [1]. On the long time scale $\tau \gg \tau_R$, the behavior is also expected to be diffusive with diffusion coefficient $D_L(Q) \equiv \lim_{\tau \gg \tau_R} D(Q,\tau)$ [1]. Since on the long time scale the movements of the particles are hindered by direct interparticle interactions, $D_L(Q) < D_S(Q)$.

We now concentrate on times such that $\tau \ll \tau_R$, when the colloidal particles hardly move and their positions can be considered fixed. Structural and hydrodynamic effects can then be separated by introducing the time-dependent hydrodynamic function $H(Q,\tau)$ so that [1]

$$\frac{D(Q,\tau)}{D_0} = \frac{H(Q,\tau)}{S(Q)} \ . \tag{3}$$

$H(Q,\tau)$ represents purely hydrodynamic effects, the structural effects being contained in the static structure factor $S(Q)$. In the absence of hydrodynamic interactions $H(Q,\tau)=1$. Following from Eqs. (1)–(3), an explicitly expression for $H(Q,\tau)$ is obtained [1]

$$H(Q,\tau) = (N D_0 Q^2)^{-1} \times \sum_{i,j} \langle \mathbf{Q} \cdot \mathbf{D}_{ij}(\tau) \cdot \mathbf{Q} \exp\{ i\mathbf{Q} \cdot [\mathbf{r}_i(0) - \mathbf{r}_j(0)] \} \rangle \ , \tag{4}$$

where the time-dependent diffusion tensors $\mathbf{D}_{ij}(\tau)$ are defined as the dyadics

$$\mathbf{D}_{ij}(\tau) = \int_0^\tau \langle \mathbf{v}_i(t') \mathbf{v}_j(0) \rangle dt' \ . \tag{5}$$

The average $\langle\ \rangle$ in expression (5) is over the velocities $\mathbf{v}_i$ of the particles, their positions being assumed fixed. This is also the reason for using the *equal-time* relative positions $\mathbf{r}_i(0) - \mathbf{r}_j(0)$ in Eq. (4).

DLS measurements are sensitive to time scales such that $\tau > \tau_B$. In order to avoid measuring the dynamics on time scales where the particles already interact directly, the short-time diffusion coefficient $D_S(Q)$ is obtained from the *initial* decay of $f(Q,\tau)$, Eq. (2),

$$D_S(Q) = \lim_{\tau \to 0} D(Q,\tau) \ . \tag{6}$$

The limit $\tau \to 0$ is meant to be taken on the time scale $\tau_B \ll \tau \ll \tau_R$. The time-independent hydrodynamic factor $H(Q)$ is then defined as $\lim_{\tau \to 0} H(Q,\tau)$ so that, from Eqs. (3) and (6),

$$\frac{D_S(Q)}{D_0} = \frac{H(Q)}{S(Q)} \ . \tag{7}$$

In the LBE simulations, fixed equilibrium configurations of particles are considered, $\mathbf{r}_i(\tau) = \mathbf{r}_i$, as we are interested in the short-time regime. This has an effect that no direct interactions between the hard-sphere particles are possible and the Brownian long-time regime is suppressed. Since the fully time-dependent hydrodynamic interactions are simulated with this method and the time-dependent hydrodynamic factor $H(Q,\tau)$ is measured, $H(Q)$ is obtained as the plateau value of $H(Q,\tau)$ when the hydrodynamics have fully developed,

$$H(Q) = \lim_{\tau \to \infty} H(Q,\tau) \ . \tag{8}$$

Then Eq. (7) can be used to determine the short-time diffusion coefficient. The ensemble averages in the calculation of $H(Q,\tau)$ are easily evaluated as averages over a set of different equilibrium particle configurations.

III. EXPERIMENT

The suspensions used in most of these studies comprised colloidal spheres of PMMA dispersed in *cis*-decalin (samples SMU33 and SMU34). The particles were stabilized sterically by thin, chemically grafted layers of poly-(12 hydroxystearic acid) (PHSA) and were prepared by the method described previously [26]. The radii of the particles were 178 nm (SMU33) and 301 nm (SMU34) (see Sec. III B 2 and Table I). The polydispersity of each preparation was approximately 0.05 (see Sec. III B 3).

Cis-decalin was chosen as a solvent because it disperses the particles well and is not measurably absorbed by them. However the refractive indices of *cis*-decalin, $n \approx 1.48$, and PMMA, $n \approx 1.50$, are sufficiently different that concentrated suspensions are visibly turbid and the TCDLS multiple scattering suppression technique is necessary to perform the light scattering measurements. The combination of samples that scatter light strongly and the TCDLS technique allows the collection of data of high accuracy. The strong scattering by the particles dominates stray scattering by dust and the sample cell walls and the TCDLS method suppresses the inevitable multiple scattering.

For the self-diffusion studies described in Sec. V C, where measurements were made at scattering vectors near the minimum of the single-particle form factor, it was necessary to use samples that gave rise to less multiple scattering. This was achieved by dispersing the particles (SMU30, radius 240 nm) in a mixture of *cis*-decalin and tetralin ($n \approx 1.54$) with a ratio of approximately 0.58/1 by weight of tetralin to *cis*-decalin. This mixture is designed to match closely the refractive index of the PMMA particles, resulting in nearly transparent samples. Tetralin was avoided for the other studies reported here because we found that particles dispersed in it showed some signs of swelling, the radius increasing by 1–2 % over several days.

In Sec. III A we describe the TCDLS technique. Section III B deals with the determination of the suspensions' volume fractions by reference to the hard-sphere "freezing" transition. In Sec. III C we describe the determination of the particles' radii by various light scattering

methods and demonstrate consistency between the results.

A. TCDLS light scattering technique

The measurements were performed with a two-color dynamic light scattering apparatus manufactured by ALV-Laser Vertriebsgesellschaft, Langen, Germany. TCDLS is a relatively new technique that allows the single-scattering function $f(Q,\tau)$ to be measured for samples that also exhibit significant multiple scattering. A complete description and demonstration of the technique has been given elsewhere [23]. Here we summarize the details relevant to the present work.

Illuminating blue ($\lambda_B = 488$ nm) and green ($\lambda_G = 514.5$ nm) beams from argon ion lasers cross at a small angle in the center of the sample, contained in a cylindrical cell. Blue light and green light, scattered from the center of the sample, are detected by separate photomultiplier tubes in directions separated by the same angle. The geometry of the incident and scattered beams is arranged precisely so that the scattering vectors associated with both blue and green scattering are *identical*, i.e., $\mathbf{Q}_B = \mathbf{Q}_G = \mathbf{Q}$. The outputs of the phototubes are then cross correlated to give

$$g_c^{(2)}(Q,\tau) \equiv \langle I_B(Q,0) I_G(Q,\tau) \rangle / \langle I_B(Q) \rangle \langle I_G(Q) \rangle , \quad (9)$$

where I is the intensity of scattered light.

With this optical arrangement, *single-scattered* light of each color probes exactly the same spatial Fourier component of the sample's density fluctuations. Thus the temporal fluctuations of each single-scattered signal are correlated, i.e., they exhibit the same fluctuations. It is not difficult to show [23] that for *double* and *higher-order* multiple scattering this degeneracy is broken. The multiple-scattered light of different colors probe different spatial Fourier density components of the sample and exhibit uncorrelated temporal fluctuations. Thus multiple-scattered light of one color is not correlated with single-scattered light of the same color or with single- or multiple-scattered light of the other color. The net result is that the time-dependent part of the intensity cross-correlation function Eq. (9) of a turbid sample reflects only the single scattering function $f(Q,\tau)$. Multiple scattering simply contributes to the time-independent "base line" of $g_c^{(2)}(Q,\tau)$.

These results can be summarized by the expression [23]

$$g_c^{(2)}(Q,\tau) = 1 + \beta_{MS}^2 \beta_{ov}^2 \beta_0^2 |f(Q,\tau)|^2 . \quad (10)$$

Here β_0^2 is the usual DLS coherence factor, which depends on the ratio of the area of the detector pinholes to the coherence area for single scattering. The factor β_{ov}^2 reflects the incomplete overlap of the two scattering volumes. The effect of multiple scattering is given by the factor β_{MS}^2, which is equal to the square of the ratio of the intensity of single-scattered light to that of the total (single plus multiple) scattered light. If multiple scattering completely dominates single scattering, $\beta_{MS}^2 \approx 0$. Clearly, for the TCDLS technique to work in practice, it is necessary that the sample is not too turbid.

We used quite small detector pinholes, giving $\beta_0^2 \approx 0.95$. The overlap factor β_{ov}^2 was typically 0.8. To minimize multiple scattering we used sample cells of inner diameter of 1 mm rather than the more standard 8-mm cells. The fraction of the intensity of light transmitted through concentrated samples in these cells was typically 0.25–0.5, indicating significant but not dominant multiple scattering. The range of scattering vectors Q studied was restricted to the region $QR < 4.0$ (where R is the radius of the particles). These values are significantly smaller than that, $QR \approx 4.49$, where the single-scattering form factor $P(Q)$ of homogeneous spheres has its first zero and there is enough single scattering from the samples for the TCDLS technique to work. For $QR > 4.0$ we found $\beta_{MS}^2 < 0.1$ and very long measurement times would have been necessary to obtain data of the necessary statistical accuracy. At scattering vectors corresponding to the main peaks in the samples structure factors we found $\beta_{MS}^2 \approx 0.6$, indicating a rather low proportion, approximately 20%, of multiple scattering in the total detected intensity. This was verified by measuring the intensity *autocorrelation* functions from either of the detectors, which showed significant distortions due to multiple scattering. Complications due to multiple scattering also prevented us from measuring accurately the static structure factors $S(Q)$ of the samples. Thus we use the theoretical Percus-Yevick expression, with the Verlet-Weis correction [25], for the structure factor of an assembly of hard spheres where necessary [for example, to use Eq. (7) to convert the measured $D_S(Q)$ to the hydrodynamic factor $H(Q)$].

Figure 1 shows several typical correlation functions $f(Q,\tau)$ obtained from a concentrated PMMA suspen-

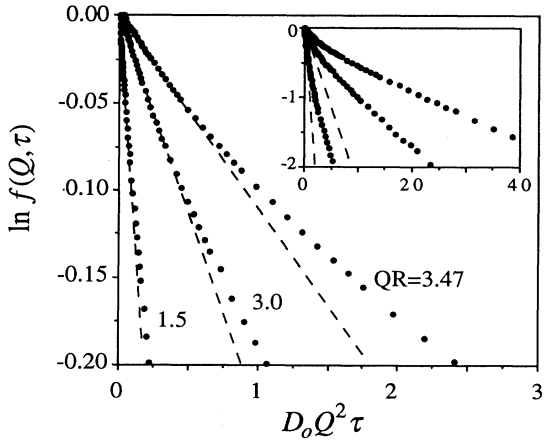

FIG. 1. TCDLS correlation functions $\ln f(Q,\tau)$ versus the normalized delay time $D_0 Q^2 \tau$ for a concentrated ($\phi = 0.472$) suspension of PMMA particles in *cis*-decalin. The values of QR are as indicated, with $QR = 3.47$ corresponding to the main peak of the structure factor $S(Q)$. Short-time diffusion is evidenced by the initial exponential decay, marked by the dashed lines. $D_S(Q)$ is extracted from cumulant fits to the data for the initial decay. Inset: $\ln f(Q,\tau)$ at longer times beyond the initial decay.

sion. Each function is an average of three experimental runs typically of 10–20 minutes in duration. The main part of the graph highlights the initial decay of $f(Q,\tau)$. This is the region of short-time Brownian diffusion, evidenced by the initial exponential decay. The data are plotted in such a way that the Q dependence of $D_S(Q)$ can be explicitly seen: the slope of a dashed line is $-D_S(Q)/D_0$ and it can be seen that the diffusion coefficients decrease near the main peak of the structure factor $QR \approx 3.5$.

The diffusion coefficients $D_S(Q)$ are calculated from the first cumulants of $f(Q,\tau)$ [27]. Care must be taken in the cumulant fits because of the visible curvature of $\ln f(Q,\tau)$ at intermediate times. The procedure used was to perform a series of fits over varying ranges of time. In this way, as the time range is decreased, the extracted value of the first cumulant is found to converge to a constant value in the region $\tau_B \ll \tau < \tau_R$ from which we determine $D_S(Q)$. The error bars given for the experimental data presented in this paper represent the standard deviation of the average of typically three separate experiments.

The inset of Fig. 1 shows the behavior of $f(Q,\tau)$ at long times $\tau > \tau_R$. We remark here that we have found that $f(Q,\tau > \tau_R)$ can also be well described by an exponential decay in time. This leads to the definition of a long-time diffusion coefficient $D_L(Q)$, an analysis of which is planned to be given in a future paper [22].

B. Sample characterization

1. *Volume fraction determination*

We evaluate the volume fraction ϕ of the colloidal sample by comparison with a fluid of hard spheres (HS's) in an *equivalent thermodynamic state*. This is done by exploiting the disorder-order transition (i.e., freezing or crystallization) observed in both HS and PMMA systems [1,28].

In our nearly monodisperse samples, homogeneous nucleation of colloidal crystallites occurs over a range of volume fractions $\Delta\phi \approx 0.08$, from the freezing transition at ϕ_f, to the glass transition at ϕ_g. However, there is a limited range $\Delta\phi \approx 0.05$ over which the colloidal crystallites and the amorphous colloidal fluid coexist. Thus we identify the limits of the range in volume fraction for which fluid-crystal coexistence is seen with the freezing and melting concentrations of HS fluids, $\phi_f = 0.494$ and $\phi_m = 0.545$ [29].

We now describe the procedure by which we prepared samples and determined volume fractions. First, a stock solution of a moderately high (not necessarily known) volume fraction is centrifuged down until it consists of a dense amorphous sediment, assumed to be near random close packing $\phi \approx 0.64$ and a clear supernatant devoid of particles. The clear supernatant is removed and solvent added so that the sample is somewhere in the fluid-crystal coexistence region $0.494 < \phi_{cx} < 0.545$. After vigorous shaking to redisperse the sediment, the sample is left to stand. Gradually, small crystallites form by homogeneous nucleation that, due to gravity, gently settle to the bottom of the sample cell. After 1 or 2 days, two visibly distinct regions appear, colloidal crystals on the bottom and amorphous colloidal fluid on top. When no further crystallites are visible in the fluid layer, the crystallization process is considered complete and the sample has reached its equilibrium thermodynamic state. At this point the heights of the crystal region h_X and of the total sample h_T are measured (see Ref. [30] for a careful analysis of the slow time-dependent gravitational settling and compression of the crystallites). Using the ideal HS freezing and melting concentrations as described above, the volume fraction of the sample in coexistence ϕ_{cx} is calculated from

$$\phi_{cx} = \phi_f + (\phi_m - \phi_f)\frac{h_X}{h_T} = 0.494 + (0.051)\frac{h_X}{h_T} . \quad (11)$$

For these DLS studies, we studied only colloidal fluid samples. These are prepared by diluting down a fluid-crystal sample prepared as above by adding some solvent of mass δ_m. A simple argument based on the addition of volumes leads to the expression for the fluid sample volume fraction ϕ

$$\phi = \frac{\phi_{cx}}{1 + \delta_m / M_T[(\tilde{\rho}/\rho_S - 1)\phi_{cx} + 1]} . \quad (12)$$

Here M_T is the total mass of the sample, ρ_S is the density of the solvent *cis*-decalin, and $\tilde{\rho}$ is the effective density of the PMMA core and the stabilizing polymer shell. At $T = 20\,^{\circ}\mathrm{C}$, $\rho_S = 0.896$ g/cm^3 and $\tilde{\rho} \approx 1.18$ g/cm^3. It is also worth emphasizing that, unlike the weight to volume fraction conversion techniques sometimes used in colloidal suspensions, at no point do we need knowledge of the individual particle sizes or volumes. The above method was also employed for the *cis*-decalin plus tetralin samples (SMU30) used for the determination of the self-diffusion coefficient D_S^S.

We now discuss the various sources of error $\delta\phi$ in the determination of the volume fractions. For ϕ_{cx}, the only source of error is in measuring the heights h_X and h_T. We estimate $\delta\phi_{cx} < \pm 0.003$. For the fluid samples, ϕ involves δ_m, M_T, and ρ_S, all of negligible uncertainty for our purposes. The only source of error is in the remaining variable, the average particle density $\tilde{\rho}$. Although the core (PMMA) and shell (PHSA) densities are known, the degree of solvation of the PHSA stabilizing hair as well as its average extension are not completely determined. However, because of the small contribution, approximately 20%, of the shell to the total particle volume as well as the closeness of the PHSA and *cis*-decalin densities, even the extreme cases, i.e., completely solvated or completely unsolvated shell, lead to small uncertainties in ϕ, of the order of $\delta\phi < 0.003$ for $\phi < 0.20$ and $0.4 < \phi < 0.494$ and $\delta\phi < 0.006$ for $0.20 < \phi < 0.40$.

2. *Mean radius*

One of the aims of comparing experimentally measured particle dynamics of PMMA spheres with those of hard-spherical colloidal particles measured by the computer simulations is to determine to what extent the PMMA particles mimic the behavior of true hard spheres. It is to

be remembered that these particles are not solid spheres of PMMA; rather they are composed of a hard PMMA core with a stabilizing PHSA layer approximately 8% of the total particle diameter in thickness [26]. One critical way of examining the nature of the particles *vis-à-vis* hard spheres is to compare measurements of the mean particle size via a range of light scattering techniques methods, each *probing a different property* of the particles.

Method 1, DLS by dilute samples, measures the viscous drag of an isolated sphere and yields the *hydrodynamic radius.* In very dilute samples, an analysis of $f(Q,\tau)$ using Eqs. (2) and (6) yields Q- and τ-independent diffusion coefficients (see, however, Sec. III B 3 below) from which intensity weighted hydrodynamic radii R_w are extracted using the Stokes-Einstein relation $D_0=k_BT/6\pi\eta_0R_w$. The viscosity η_0 of *cis*-decalin is $\eta_0=3.381$ cp at $T=20\,^{\circ}\mathrm{C}$, as measured in our laboratory with an Ubbelhode viscometer. The number average radius R, of interest here and listed in Table I, is slightly smaller than R_w, $R=R_w/(1+5\sigma^2)\approx 0.988R_w$, due to a slight particle size polydispersity $\sigma\approx 0.05$ [31].

Method 2 uses conventional light scattering by dilute samples to determine the size by comparing the measured single particle scattering form factor $P(Q)$ with that expected for hard spheres [6]. In particular, a mean radius can be obtained by comparing the position of the first experimental minimum in $P(Q)$ at $Q_{\min}^{\mathrm{expt}}$ with the theoretical result $(QR)_{\min}^{\mathrm{theor}}=4.49$.

The next two methods determine particle radii from a comparison of measured and theoretical (hard sphere) structure factors $S(Q)$ in dense fluids and colloidal crystals. Previous work on similar suspensions has shown that HS models can well describe the experimental results for $S(Q)$ in PMMA suspensions [1]. A further comparison of the experimental and theoretical static structure factors is not done here. Rather, our aim is simply to extract an effective hard-sphere radius, denoted here as the *hard-sphere interaction radius,* by identifying the experimental value of the position of the main peak Q_m^{expt} with the theoretical values $(QR)_m^{\mathrm{theor}}$. The first of these two methods, method 3, is to measure the intensity $I(Q)$ of light scattered by a fluid sample at the freezing transition $\phi=0.494$ and relate it to the structure factor $S(Q)$ via the relation

$$I(Q)\propto P(Q)S(Q)\ . \tag{13}$$

Here $P(Q)$ is the measured single-particle form factor and this relation is valid for monodisperse spheres. From $S(Q)$, a mean particle radius R is extracted using the theoretical Percus-Yevick (Verlet-Weis) result of $(QR)_m^{\mathrm{theor}}\sim 3.47$ for HS fluids [25]. Finally, in method 4, the intensity $I(Q)$ [and hence $S(Q)$] scattered by the sedimented colloidal crystal ($\phi=0.545$) in a coexisting fluid-crystal sample is measured. It is known that colloidal crystallites form a random-stacked, close-packed lattice structure with a strong Bragg scattering peak at $(QR)_{\mathrm{Bragg}}\approx 3.475$ [1] so that the mean radius can be determined.

We now discuss the results listed in Table I. For each of the three sets of particles, there is close agreement between the mean particle sizes measured using the four different techniques. Most values agree to within the quoted errors, all of which are less than 2%. Evidence for the hard-sphere-like nature of particles is perhaps best given by the close agreement of the radii determined by the *hydrodynamic* method, 1, and the *hard-sphere interaction* methods, 3 and 4. The presence of either attractive or repulsive forces between particles or of deformation of the PHSA polymer layer under interparticle contact could lead to significant differences between these two measurements. Given that all four methods yield the same radii within errors, we note that the last method, involving the crystalline Bragg peak in a coexisting sample, has many advantages over the others. The volume fraction is known exactly, yielding $(QR)_{\mathrm{Bragg}}\approx 3.475$, and the Bragg peak is sharply defined and easily measured. In addition, the lattice spacing is relatively insensitive to polydispersity and the solvent viscosity does not need to be known.

3. *Polydispersity*

In Sec. V we will compare results from experiments and computer simulations for particle dynamics in concentrated suspensions. We point out that there is an important difference between the two systems involved in this comparison: the PMMA spheres are slightly polydisperse in size while the LBE particles are practically monodisperse (to within 0.5%; see the discussion in Sec. IV). Thus disagreements between the results of experiment and theory could reflect the effects of polydispersity.

The polydispersity of the particles was measured by TCDLS on dilute samples using the method of Pusey and van Megen [31], in which the average diffusion coefficient

TABLE I. PMMA particle size determination.

Method	Measured	Name	Relation	SMU33 (nm)	SMU30 (nm)	SMU34 (nm)
1	D_0	dilute DLS	$R=[k_BT/6\pi\eta_0D_0]/(1+5\sigma^2)$	180±2	240±4	303±3
2	$P(Q)$	dilute min.	$(QR)_{\min}^{\mathrm{theor}}/Q_{\min}^{\mathrm{expt}}$	178±3	235±4	302±4
3	$S(Q)$	conc. peak	$(QR)_m^{\mathrm{theor}}/Q_m^{\mathrm{expt}}$	176±2	239±3	299±3
4	$S(Q)$	crystal peak	$(QR)_{\mathrm{Bragg}}^{\mathrm{theor}}/Q_{\mathrm{Bragg}}^{\mathrm{expt}}$	176±2	246±2	300±3
			Average	178±2	240±4	301±2

$D_S(Q)$ describing the (nearly exponential) decay of the intermediate scattering function is measured as a function of Q. Near the minimum in the particles' average form factor, $D_S(Q)$ shows a characteristic "swing" as first the large particles and then the small ones scatter weakly. For narrow, reasonably symmetrical size distributions, the peak-to-peak amplitude of the swing is twice the particle polydispersity σ. Figure 2 shows the results for the SMU33 particles. These measurements give $\sigma \approx 0.05$.

Since the theory is not well developed, we can only speculate about the effects of particle polydispersity on the dynamics of concentrated suspensions. Equation (7) relates $D_S(Q)$ to the hydrodynamic and static structure factors $H(Q)$ and $S(Q)$. There are theories for the static structure factor of suspensions of polydisperse hard spheres, e.g. [32], that predict that, for $\sigma = 0.05$, the amplitudes of the main peak $S(Q_m)$ are reduced by 1%, 2%, and 5% for volume fractions $\phi = 0.25$, 0.35, and 0.45, respectively, compared to the values for a monodisperse system. The effect of polydispersity is thus small, but not negligible. However, there appear to be no predictions for the effect of polydispersity on $H(Q)$. Here we simply note that the good agreement found in Sec. V between the experimental results for a slightly polydisperse system and the simulations for an effectively monodisperse system implies that polydispersity affects $H(Q)$ and $S(Q)$ in much the same way, leading to cancellation in Eq. (7).

IV. FLUCTUATING LATTICE BOLTZMANN SIMULATIONS

A. Simulation technique

The numerical simulation method used in this paper is based upon the combinations of Newtonian dynamics for the solid particles with a fluctuating lattice Boltzmann equation for the suspending fluid [18–20]. The principal advantage of this method over conventional algorithms for simulating colloidal suspensions, such as Brownian dynamics with hydrodynamic interactions [12] or the multipole method [13], is that it simulates the *time-dependent* hydrodynamic interactions. Therefore, while conventional algorithms assume that the hydrodynamic interactions are fully established and *global,* depending on the positions and velocities of *all* the particles, the LBE algorithm simulates the development of the interactions from purely *local* forces at the solid-fluid interface that then diffuse throughout the fluid. This fundamental difference results in the LBE algorithm scaling lincarly with the number of particles and, although some allowance in computational time has to be made for the time-evolution of the flow if *steady-state* solutions are to be reached, the LBE method represents a considerable improvement over conventional algorithms, which scale mostly as the cube of the number of particles.

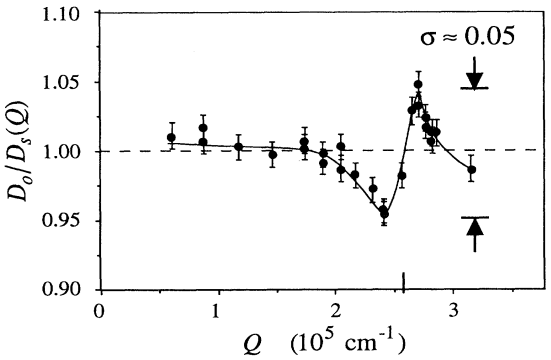

FIG. 2. Determination of PMMA particle size polydispersity σ using TCDLS in a dilute sample $\phi < 0.01$. D_0 is the (number average) free-diffusion coefficient. The minimum of the form factor $P(Q)$ is denoted by the line at $QR \sim 2.6 \times 10^5$ cm^{-1} and the solid line is a guide to the eye. The polydispersity $\sigma \approx 0.05$ is obtained from the amplitude 2σ of the peak-to-peak variation in $D_0/D_S(Q)$ (see the text).

The lattice Boltzmann equation method has emerged in recent years as a powerful tool to simulate fluid flows [33,34]. It is based on the well established connection, described by kinetic theory, between the dynamics of a dilute gas and the Navier-Stokes equation [35]. In the LBE method, space is spanned by a regular lattice and the allowed velocities of the "gas" particles are restricted to a set $\{\mathbf{c}_i\}$, $i = 1, \ldots, n$. The $\mathbf{c}_i$ link a lattice node $\mathbf{r}$ to a set of neighboring lattice nodes. The fundamental quantity is the particle distribution function $f_i(\mathbf{r},t)$, describing the probability of finding a gas particle at lattice site $\mathbf{r}$, time t, and with velocity $\mathbf{c}_i$. The hydrodynamic fields, the density $\rho(\mathbf{r},t)$, and momentum density $\rho(\mathbf{r},t)\mathbf{u}(\mathbf{r},t)$ are defined as velocity moments of the distribution function

$$\rho(\mathbf{r},t) = \sum_{i=1}^{n} p_i f_i(\mathbf{r},t) , \tag{14}$$

$$\rho(\mathbf{r},t)\mathbf{u}(\mathbf{r},t) = \sum_{i=1}^{n} p_i f_i(\mathbf{r},t)\mathbf{c}_i , \tag{15}$$

where $\mathbf{u}(\mathbf{r},t)$ is the hydrodynamic velocity of the fluid and the p_i are weights associated with velocity direction $\mathbf{c}_i$. At each time step, the distribution functions are propagated along $\mathbf{c}_i$ to the next lattice site where a collision process takes place [33,34]. In the present implementation of the method, the collision process is chosen to be the simplest possible: the distribution functions are relaxed to their local equilibrium $f_i^{\mathrm{eq}}(\mathbf{r},t)$ with a relaxation parameter τ_{BGK}. This is the so-called Bhatnagar-Gross-Krook (BGK) method [36,37]. The time evolution of the distribution function is thus described by the kinetic equation

$$f_i(\mathbf{r}+\mathbf{c}_i, t+1) = f_i(\mathbf{r},t) - \frac{f_i(\mathbf{r},t) - f_i^{\mathrm{eq}}(\mathbf{r},t)}{\tau_{\mathrm{BGK}}} . \tag{16}$$

The choice of τ_{BGK} determines the viscosity of the fluid and is restricted to $\tau_{\mathrm{BGK}} > \frac{1}{2}$. It can be shown that, subject to an appropriate choice of the equilibrium distribution and the underlying lattice (including the weights p_i), the hydrodynamic fields ρ and $\rho\mathbf{u}$ obey the incompressible Navier-Stokes equations in a small Mach number, small Knudsen number approximation [33,34].

Flows in colloidal suspensions occur at low Reynolds number and can be described by the linearized Navier-Stokes equation. The local equilibrium distribution $f_i^{eq}(\mathbf{r},t)$ is thus chosen such that the nonlinear terms in the Navier-Stokes equation vanish [33]

$$f_i^{eq}(\mathbf{r},t)=\frac{\rho(\mathbf{r},t)}{b}\left[1+\frac{K}{c^2}\mathbf{u}(\mathbf{r},t)\cdot\mathbf{c}_i\right] . \tag{17}$$

Here b, K, and c^2 are lattice-dependent parameters.

To simulate the thermal fluctuations in the fluid driving the Brownian motion of the solid colloidal particles, stochastic terms f_i' are added to the distribution functions f_i of the LBE fluid in such a way that they do not alter the density ρ or momentum density $\rho\mathbf{u}$, but add a fluctuating component to the stress tensor σ of the fluid [18,19]. The stress tensor is defined as

$$\sigma(\mathbf{r},t)=\sum_{i=1}^{n} p_i f_i(\mathbf{r},t)\mathbf{c}_i\mathbf{c}_i \tag{18}$$

and the random stress fluctuations $\sigma'=\sum_i p_i f_i'\mathbf{c}_i\mathbf{c}_i$ are δ-correlated in space and time [38]

$$\begin{aligned}\langle\sigma'_{\alpha\beta}(\mathbf{r}_1,t_1)\sigma'_{\gamma\delta}(\mathbf{r}_2,t_2)\rangle &= A\,\delta(\mathbf{r}_1-\mathbf{r}_2)\delta(t_1-t_2)\\ &\times[\delta_{\alpha\gamma}\delta_{\beta\delta}+\delta_{\alpha\delta}\delta_{\beta\gamma}-\tfrac{2}{3}\delta_{\alpha\beta}\delta_{\gamma\delta}] .\end{aligned} \tag{19}$$

The variance A can be linked via a fluctuation-dissipation theorem to the effective temperature and the viscosity of the fluid [19].

An important part of the simulations of colloidal suspensions is the mechanism of interaction between the particles and the fluid via the so-called boundary rules. In a recent paper [20], we have introduced a set of boundary rules that, while identical in effect, are somewhat simpler to implement than the rules pioneered by Ladd [19]. We have also introduced some simplifications to the LBE fluid plus colloidal particles algorithm and have shown that this method reproduces the dissipative and fluctuating hydrodynamic forces between the solid particles with good accuracy over the whole range of particle volume fractions [20]. Indeed, computations of two-particle hydrodynamic interactions have been shown to agree with independent calculations [13] down to interparticle separations of less than one lattice spacing for particle radii of only three lattice spacings [20]. Similarly, computations via both dissipative and fluctuating methods [19,20] of the self-diffusion coefficients, sensitive to the many-body hydrodynamics interactions [2], agree with independent calculations [13] for particle radii of only about four lattice spacings at the highest particle volume fractions.

In our method, a colloidal particle is mapped onto the lattice by marking the lattice nodes lying the closest to its surface as boundary nodes. Thus a discrete representation of the particles as sets of boundary nodes is obtained and this representation becomes more and more precise as the particle radius increases. We note that the positions of the centers of mass of the particles are continuous and not restricted to lie on the lattice nodes. The lattice nodes inside and outside of the particles are treated in a similar fashion. However, due to the relatively small particle volume, the interior fluid quickly relaxes to the solid-body motion of the particles and only adds an additional inertia [19]. At each time step and each boundary node $\mathbf{r}_b$, population density between opposite velocity directions $\mathbf{c}_i$ and $\mathbf{c}_{-i}=-\mathbf{c}_i$ is exchanged in such a way that the local velocity $\mathbf{u}(\mathbf{r}_b)$ of the fluid is matched to the solid-body velocity $\mathbf{u}_b$ of the particle,

$$\mathbf{u}_b=\mathbf{U}_i+\boldsymbol{\Omega}_i\times(\mathbf{r}_b-\mathbf{r}_i) . \tag{20}$$

Here $\mathbf{U}_i$ and $\boldsymbol{\Omega}_i$ are the velocity and angular velocity of particle i and $\mathbf{r}_i$ is the position of its center of mass. A hydrodynamic stick boundary condition is thus implemented at the particle surface [20]. The local fluid density is not affected by this boundary rule. The change of fluid momentum at the boundary nodes results in forces and torques onto the particles, whose translational and angular velocities are then updated according to Newtonian mechanics.

The discretization of the particles on the lattice requires the determination of an effective hydrodynamic radius that determines their size with respect to their interactions with the fluid. This radius is obtained by calculating the drag force on an array of spheres at low particle volume fraction and fitting the results to the theoretical expression of the friction coefficient by Hasimoto [39,19]. Since the particle position is continuous, several different discrete representations for a given input radius may occur, resulting in different hydrodynamic radii. We use here an average radius, obtained by averaging the hydrodynamic radii over about 100 different particle positions; the standard deviation on the average radius is not more than 0.5% [20]. The hydrodynamic radii are usually within 20% of the input radii used to map the particles onto the discrete lattice.

B. Simulations

We concentrate in this paper on the short-time limit $\tau\ll\tau_R$, when the colloidal particles hardly move and only interact via the hydrodynamic interactions. Systems of *fixed* equilibrium configurations of N hard spheres contained in a periodic box have thus been simulated. The particles being fixed, the long-time Brownian regime is suppressed and the short-time transport coefficients are obtained once the hydrodynamic interactions between the particles have been established. The configurations of particles were generated with a standard hard-sphere Monte Carlo program and our data have been obtained by averaging the results over 32–64 different equilibrium configurations per solid particle volume fraction.

We use a LBE model based on a simple cubic lattice with $n=14$ velocity directions, 6 along the (1 0 0) directions (with weight $p_i=8$) and 8 along the (1 1 1) directions (with weight $p_i=1$) [20]. For this lattice, the parameters are $b=56$, $K=7$, and $c^2=3$. A relaxation parameter $\tau_{BGK}=1$ has been used that simplifies considerably the algorithm [see Eqs. (16) and (17)]

$$f_i(\mathbf{r}+\mathbf{c}_i,t+1)=\frac{\rho(\mathbf{r},t)}{b}\left[1+\frac{K}{c^2}\mathbf{u}(\mathbf{r},t)\cdot\mathbf{c}_i\right] . \quad (21)$$

The input radii used for the simulations ranged from 2.5 lattice spacings for the most dilute suspensions to 4.0 lattice spacings for the most concentrated suspensions.

The Q-dependent diffusion coefficients have been obtained by integrating the velocity cross-correlation functions from zero to a time where the integral has reached a constant within statistical errors [see Eqs. (4), (5), (8), and (7)]. We use the Verlet-Weis [25] correction to the Percus-Yevick closure to calculate $S(Q)$. In Fig. 3 the time dependence of $D(Q,\tau)$ as the hydrodynamic interactions develop is shown. This time dependence has been the subject of recent work and interesting scaling properties have been obtained [21]. We will, however, in the present work concentrate on the steady hydrodynamics and $D_S(Q)/D_0=\lim_{\tau\to\infty}D(Q,\tau)/D_0$.

The self-diffusion coefficients D_S^S have been obtained either by integrating the velocity autocorrelation functions of the particles or by taking the high-Q limit of $D_S(Q)$. Since the simulations are done in a periodic system with a cell size $L\times L\times L$, the Q vectors have to be commensurate with this cell, i.e., $\mathbf{Q}=(2\pi/L)(n\mathbf{i}+m\mathbf{j}+l\mathbf{k})$, where $\mathbf{i}$, $\mathbf{j}$, and $\mathbf{k}$ are unit vectors on the lattice in the three dimensions and n, m, and l are integers such that $1\le n,m,l\le L$. Since $D_S(Q)$ depends only on the magnitude Q of the wave vector $\mathbf{Q}$, we have averaged it over the different combinations of the indices n, m, and l, giving the same amplitude Q.

The diffusion coefficients have a strong system-size dependence and the results reported here are extrapolations to the thermodynamic limit ($N\to\infty$) from simulations with N particles. The finite-size correction used to obtain the thermodynamic limit was proposed by Ladd [13]; since the correction is Q-vector independent, we will omit in the following development the reference to Q and denote $D(N)$ the short-time diffusion coefficient of a system of N spheres in a periodic system. The correction to $D(N)$ is obtained by first considering the diffusion of an isolated sphere in a periodic system. The friction coefficient for such a system was calculated by Hasimoto [39], who obtained the low-density expansion for the friction coefficient of a simple cubic lattice. The friction coefficient can be linked to the diffusion coefficient via the Einstein relation [1] and Hasimoto's result yields

$$D_{sc}/D_0=1-1.7601\phi^{1/3}+\phi-\cdots . \quad (22)$$

Superposing the effects from neighboring particles, one obtains an expression for $D(N)$ at low particle volume fractions [40]

$$D(N)/D_0=D/D_0-1.7601(\phi/N)^{1/3}+\phi/N . \quad (23)$$

Here D is the thermodynamic limit $D=D(N\to\infty)$. At higher particle volume fractions, the effects from the periodic images are partially screened by neighboring particles. To take account of this effect, the viscosity η_0 of the pure fluid is replaced with the high-frequency suspension viscosity η and thus [13]

$$\begin{aligned} &D/D_0=D(N)/D_0+D_{\rm corr}(N)/D_0 ,\\ &D_{\rm corr}(N)/D_0=(\eta/\eta_0)[1.7601(\phi/N)^{1/3}-\phi/N] . \end{aligned} \quad (24)$$

To determine the suspension viscosity, we use an expression proposed by Bedeaux [41]

$$\frac{\eta/\eta_0-1}{\eta/\eta_0+3/2}=\phi[1+R(\phi)] . \quad (25)$$

An empirical expression for the virial expansion of $R(\phi)$ to third order in ϕ has been obtained by Ladd to fit both his numerical results [13] and the experimental data of van der Werff *et al.* [42]:

$$R(\phi)=\phi+\phi^2-2.3\phi^3 . \quad (26)$$

We demonstrate in Fig. 4 the effectiveness of the correction by showing the finite-size corrected inverse short-time diffusion coefficient $D_0/D_S(Q)$ for three different system sizes ($N=16$, 32, and 108 particles) at the same particle volume fraction ($\phi=0.443$). The corrected results can be seen to be almost identical for the three system sizes. The corrections at this volume fraction are $D_{\rm corr}(16)/D_0=0.095$, $D_{\rm corr}(32)/D_0=0.077$, and $D_{\rm corr}(108)/D_0=0.053$. These corrections are certainly not negligible, especially in the vicinity of the peak in $D_S(Q)$, where the smallest value of $D_S(Q)/D_0\approx 0.175$ is found.

We have used a system size of $N=32$ for all the results presented in the following comparison with experiments. The error estimates are standard deviations to the average of simulations of 32–64 different particle configurations.

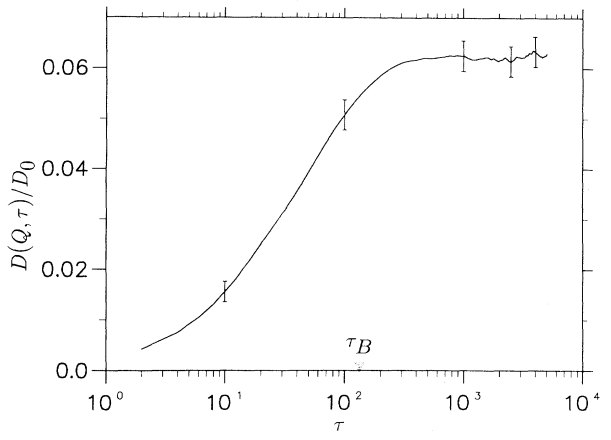

FIG. 3. LBE simulation results for the time-dependent diffusion coefficient $D(Q,\tau)$ normalized by the isolated-sphere result D_0. The development of the short-time Brownian motion is clearly seen and the short-time diffusion coefficient $D_S(Q)$ is identified as the plateau value $D(Q,\tau\to\infty)$. τ_B is the Brownian relaxation time, the characteristic time scale for the decay of the particle velocity correlation functions. Simulation of 32 particles at volume fraction $\phi=0.491$ for $Q=Q_m$, at the peak in the structure factor.

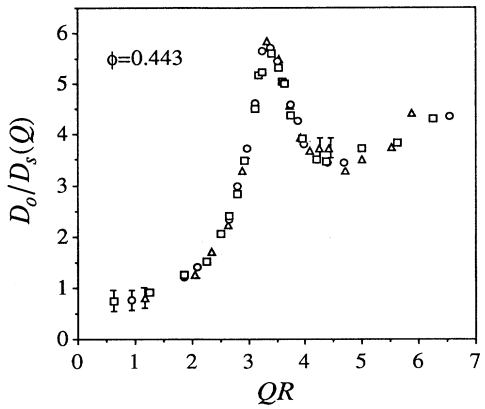

FIG. 4. Demonstration of the finite-size correction in the LBE simulations. The finite-size-corrected Q-dependent inverse diffusion coefficients $D_0/D_S(Q)$, normalized by the isolated-sphere result D_0, are plotted versus QR for simulations of 16 (open squares), 32 (open circles), and 108 (open triangles) particles.

V. RESULTS AND DISCUSSION

We now present the results of the TCDLS experiments and the LBE simulations. Separate sections are devoted to the general Q-dependent diffusion coefficient $D_S(Q)$, the peak diffusion values $D_S(Q_m)$, where Q_m is the wave vector for which the structure factor $S(Q)$ is maximum, the short-time self-diffusion D_S^S, and the short-time collective diffusion D_S^C.

A. Q-dependent diffusion

Figures 5(a)–5(d) show our results for the inverse normalized diffusion coefficients $D_0/D_S(Q)$ versus QR from both experiment and simulation. Here D_0 is the isolated-sphere diffusion constant $D_0=k_BT/6\pi\eta_0R$. The radius R used for the PMMA suspensions is that listed as the average radius in Table I.

All the plots have shapes reminiscent of the static structure factor $S(Q)$ [see Fig. 5(d)], in agreement with previous work [7]. The smallest diffusion coefficients, corresponding to the slowest decay of the density fluctuations, are observed at Q vectors close to where $S(Q)$ has its main peak $Q=Q_m$. While in the vicinity of the peak the diffusion is always slower than free diffusion, this is not the case for $Q \ll Q_m$, where the diffusion actually speeds up. This is due to collective motions of neighboring particles that allow for a fast decay of the long-wavelength fluctuations.

For all volume fractions presented in Figs. 5(a)–5(d), excellent quantitative agreement is found between the TCDLS experiments on PMMA suspensions and the LBE computer simulations of hard spheres. The solid lines shown are the theoretical results of Beenakker and Mazur [2]. Good agreement is found at $\phi=0.30$, less so at $\phi=0.382$. For the higher volume fractions, while the general shape of the data is well reproduced by the

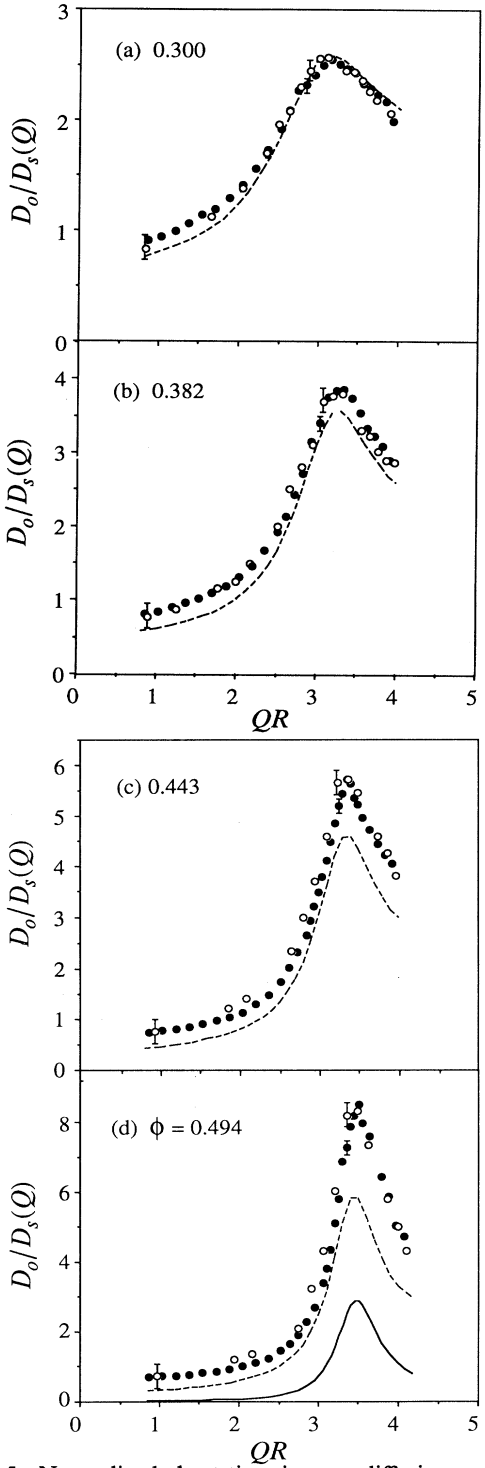

FIG. 5. Normalized short-time inverse diffusion coefficients $D_0/D_S(Q)$ versus QR for four different particle volume fractions. The closed circles represent TCDLS experiments on particles of PMMA (SMU33), the open circles are LBE simulations, and the dashed lines the theoretical predictions of Beenakker and Mazur [2]. The solid line in (d) is the theoretical static structure factor $S(Q)$. The volume fractions listed apply to experiment and theory; the corresponding volume fractions for the simulations were (a) 0.311, (b) 0.382, (c) 0.443, and (d) 0.491.

theory, it consistently overestimates the diffusion coefficients. These observations agree with the estimated range of validity of the theory; at low Q, Beenakker and Mazur are reluctant to quote values for $D_S(Q)$ for $\phi \geq 0.30$ [2], while for intermediate and large wave vectors, the theory is expected to be valid up to $\phi \sim 0.35-0.40$.

We now turn to the effects of the solvent mediated hydrodynamic interactions, remembering that, while $D_S(Q)$ depends on both hydrodynamic and structural effects, $H(Q)$ is a purely hydrodynamic quantity [see Eq. (7)]. In experimental systems where hydrodynamic interactions are negligible, such as suspensions of charged colloidal particles with sufficiently long-range repulsions [1] or theoretical models and simulations that neglect these interactions, the hydrodynamic factor $H(Q)=1$ and $D_0/D_S(Q)=S(Q)$. In Fig. 5(d) we have plotted alongside our data for $D_S(Q)$ the structure factor $S(Q)$. It is apparent from this figure that the neglect of the hydrodynamic interactions would lead to significantly different results. It is evident that the overall effect of the hydrodynamic interactions is to slow down the diffusive motions considerably. In Fig. 6 we plot the hydrodynamic function $H(Q)$ versus QR for several concentrated suspensions. Note that, whereas the LBE simulations calculate $H(Q)$ directly (see Sec. IV B), the experimental data for $H(Q)$ were obtained from the measured diffusion coefficients $D_S(Q)$ and the Percus-Yevick expression (modified by the Verlet-Weis correction) for the structure factor $S(Q)$ [see Eq. (7)]. It is apparent that $H(Q)$ is smallest at low Q. However, since the structure factor itself is small at low Q, a considerable cancellation in the calculation of $D_S(Q)/D_0$ occurs and, as noted above, the diffusion at low Q is actually faster than that around the peak.

It is worth emphasizing here the importance of the experimental particle radius determination. As mentioned above, the values for $H(Q)$ were obtained by dividing the diffusion data of Fig. 5 by the theoretical $S(Q)$, or rather $S(QR)$. Since the form of $S(QR)$ contains in general several sharp peaks, especially at high particle volume fraction, the derived data for $H(Q)$ can change significantly upon even a few percent change in R. This problem is negligible in the LBE simulations, where the radius of the particles is known within about 0.5%. The close agreement of the experimental and computational results in Fig. 6 confirms the procedures used in determining the mean radius R as well as the coincidence of the sample structure factors with the theoretical Percus-Yevick (Verlet-Weis corrected) expression. We point out that there is a slight difference between the volume fractions of the experiments and the volume fractions of the simulations, noted in the figure captions where appropriate.

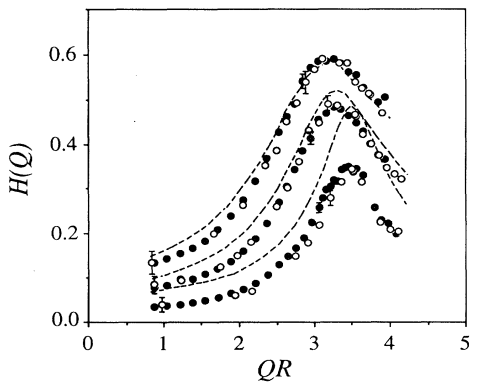

FIG. 6. Hydrodynamic factors $H(Q)$ vs QR. The data points are extracted directly from the points shown in Fig. 5 using the relation $H(Q)=S(Q)[D_S(Q)/D_0]$. The volume fractions are 0.311, 0.382, and 0.491 from top to bottom. The dashed lines are the theoretical predictions of Ref. [2].

Overall, these results give strong evidence for the success of the LBE technique to simulate the full hydrodynamic interactions in concentrated suspensions, as well as for the hard-sphere-like nature of the PMMA particles. We also gain considerable confidence in our procedure for determining the colloid volume fraction ϕ, based on the identification of the colloidal freezing transition with that of HS fluids.

B. Diffusion at the peak

In this section, we consider the diffusion coefficients for $Q=Q_m$, the wave vector for which the structure factor is maximum. For this wave vector, dynamics and structures on a length scale comparable to the nearest-neighbor interparticle distance are probed. Our experimental data confirm that for all three samples listed in Table I, the smallest diffusion coefficients $D_S(Q)$ occurred at values of Q coincident (within errors of approximately 1%) with the structure peak at $Q=Q_m$.

In Fig. 7 we present the experimental and numerical results for these values. Excellent quantitative agreement over all volume fractions up to the disorder-order transition is found. The experimental data on this graph have been obtained for two different sized particles, $R=178$ and 301 nm. In addition, the graph contains points from well over a dozen individually made samples. The agreement of the results from separately prepared samples, even at high volume fractions ϕ where there is a strong dependence of $D_0/D_S(Q_m)$ on ϕ, is an excellent indication that the quite small random errors $\delta\phi < 0.01$ estimated for the determination of the sample volume fractions are in fact reasonable.

For future reference, it may be helpful to describe the results for the diffusion coefficients at the peak by a polynomial fit, accurate to within 4% for $\phi > 0.10$,

$$D_0/D_S(Q_m)=1.0-2.0\phi+58\phi^2-220\phi^3+347\phi^4 . \quad (27)$$

An interesting observation can be made by plotting our data versus the inverse volume fraction $1/\phi$. As illustrated in the inset of Fig. 7, we found that the data can then be described by a linear function for volume fractions $\phi > 0.37$. Moreover, the extrapolated volume fraction ϕ^* of zero diffusion coefficient $D_S(Q_m)=0$ was found to be $\phi^*=0.64\pm0.01$. The errors reflect one standard devia-

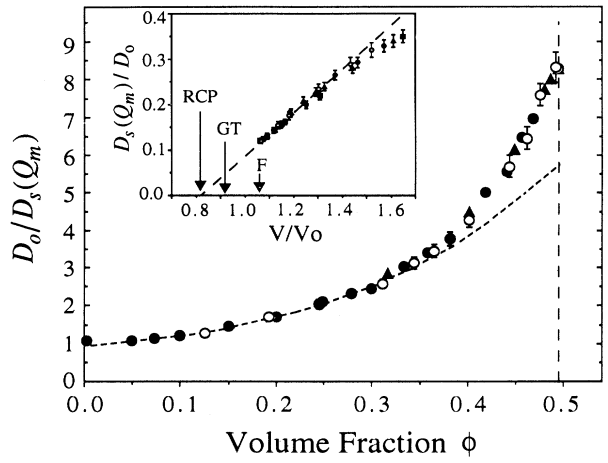

FIG. 7. Normalized short-time inverse diffusion coefficients at the main peak of the structure factor $D_0/D_S(Q_m)$ versus volume fraction ϕ. The symbols are the same as in Fig. 5, with in addition the closed triangles being TCDLS experiments on SMU34. The dashed line is the theory from Ref. [2]. The line at $\phi=0.494$ represents the disorder-order transition. Inset: The same data are plotted in the Batchinski-Hildebrand form [44], $D_S(Q_m)/D_0$ versus the reduced volume per particle $V/V_0=\pi/6\phi$, where $V_0=(2R)^3$. The arrows F, GT, and RCP stand for the reduced volumes at the freezing transition ($V/V_0=1.060$), the glass transition ($V/V_0\approx 0.91$), and random close packing ($V/V_0=0.821$). The dashed line is a best fit to all the data in the asymptotic region $V/V_0<1.4$ ($\phi>0.37$).

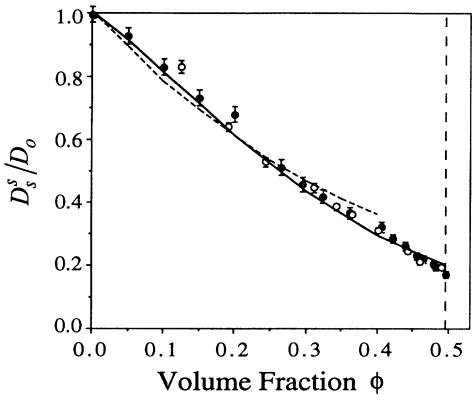

FIG. 8. Normalized short-time self-diffusion coefficients D_S^S/D_0. The symbols are the same as in Fig. 5, with the TCDLS experiments being done on PMMA particles (SMU30) in a mixture of the solvents *cis*-decalin and tetralin. The experimental data are from measurements of $D_S(Q)/D_0$ at Q such that $S(Q)\approx 1.0$ near $QR\approx 4.0$. The simulation data are from evaluations of $D_S=D(Q\rightarrow\infty)$ or from integration of the velocity *autocorrelation* function of the particles. Also shown are the theoretical results of Refs. [2] (dashed line) and [4] (solid line).

tion of the separate fitting results for the two experimental (SMU33 and SMU34) as well as the LBE numerical results. While we acknowledge that other extrapolation procedures might yield different results, it is interesting to find ϕ^* to be in agreement with the amorphous random close-packing (RCP) volume fraction $\phi_{\rm RCP}=0.638$. The physical significance of this result is not clear, but we consider it interesting enough to report it here. We also emphasize that we are considering very short-time and -distance diffusion in this work. This is in contrast to the long-time and -distance diffusion whose description for $\phi>0.5$ has been shown to be accounted for by mode-coupling theories of the glass transition [43].

C. Self-diffusion

We now consider the short-time self-diffusivity D_S^S, starting with Eq. (1) for the intermediate scattering function $F(Q,\tau)$. At large values of QR, small variations in the relative particle positions $\mathbf{r}_i(0)-\mathbf{r}_j(\tau)$ cause large variations of the phase factors $\mathbf{Q}\cdot[\mathbf{r}_i(0)-\mathbf{r}_j(\tau)]$. Thus the cross terms $i\neq j$ in Eq. (1) disappear in the ensemble average and $F(Q\rightarrow\infty,\tau)$ becomes the self intermediate scattering function $F_S(Q,\tau)\equiv\langle\exp\{i\mathbf{Q}\cdot[\mathbf{r}_i(0)-\mathbf{r}_i(\tau)]\}\rangle$. In this limit therefore DLS measures the average self-motion of individual particles and $D_S(Q\rightarrow\infty)$ becomes D_S^S [45].

The particles used in this work are too small to allow access to large enough QR to ensure the measurement of self-motions. Nevertheless we note that there are smaller values of QR, on either side of the main peak of $S(Q)$, where $S(Q)=F(Q,0)=1$ due to cancellation of the cross terms. While the absence of cross terms in the equal-time function $F(Q,0)$ does not guarantee their absence in $F(Q,\tau)$, previous work [46] has shown that $F(Q,\tau)$, measured where $S(Q)=1$, gives a reasonable description of self motions.

For all volume fractions studied, the values of $D_S(Q)$ found for $QR\sim 4.0$, $S(QR)=1$, just to the right of the main peak, are equal, to within experimental uncertainty (approximately 5%), to the computed LBE self-diffusion values D_S^S found for $QR>18$. Moreover, the LBE results at $QR\sim 4.0$, $S(QR)=1$, are also in close agreement with the values computed in the high Q limit, supporting the idea that the self-diffusion can be measured at points where $S(QR)=1$. We have also found this property to be true for the theory of Beenakker and Mazur [2]. In fact, the LBE and Beenaker-Mazur results show that *all* values of $D_S(Q)$ measured beyond the main peak in $S(Q)$ can be identified with that of self-diffusion D_S^S to within 10% for $\phi<0.35$ and 20% for $\phi<0.494$. This is not a surprising result in that this range of QR corresponds to probing length scales smaller than the average interparticle separation, where single particle contributions to $f(Q,\tau)$ should dominate.

In Fig. 8 we plot the experimental and simulation results for self-diffusion. The experimental results have been obtained, as discussed above, at $QR\sim 4.0$, $S(QR)=1$. Very good agreement is indeed seen between the TCDLS data and the LBE simulation results over the entire volume fraction range up to the freezing transition.

Both data sets also are in a good agreement with previous measurements [1] and with theoretical predictions of Tokuyama and Oppenheim [4] over this same range. The predictions of Ref. [2] work well for $\phi < 0.40$, as expected.

D. Collective diffusion

Finally, we present data for the collective diffusion coefficient $D_S^C = D_S(Q \to 0)$, which describes the decay of long-wavelength density fluctuations. While the $Q = 0$ limit can never strictly be reached in the laboratory, D_S^C is assumed to be found when $D_S(Q)$ does not vary appreciably with Q at low Q. In our light scattering measurements, shown in Fig. 5, $D_S(Q)$ was found to be still dependent on Q at the lowest values studied. An extrapolation procedure was therefore used to obtain estimates of D_S^C. In an expansion of $D_S(Q)$ in powers of Q, only even powers remain for symmetry reasons. We have found that plots of $D_S(Q)$ against Q^2 show reasonable linearity at low Q and can therefore be extrapolated to $Q = 0$ to provide the estimates of D_S^C shown in Fig. 9.

The computational data presented in this figure have not been obtained via the *fluctuating* LBE method presented in the present paper but via a purely *dissipative* LBE method [20,19]. In this method, *no* thermal fluctuations are added to the fluid; however, by solving the Stokes equations for the friction coefficients of equilibrium configurations of $N = 16$ spheres and using the Einstein relation [1], the collective diffusion coefficient can be obtained. While the non-finite-size corrected data have already been presented elsewhere [20], here we apply the size corrections described in Sec. IV B.

Also shown in Fig. 9 is the exact result obtained by Batchelor [47], taking account of all the hydrodynamic interactions in the low-ϕ limit,

$$\frac{D_S^C}{D_0} = 1 + 1.45\phi + \cdots . \tag{28}$$

As is apparent from Fig. 9, the computational data are in excellent agreement with this prediction at low ϕ, while significant deviations are observed for the experimental data. It is possible that these deviations result from the lack of data at low enough Q to provide reliable extrapolation to $Q = 0$. Nevertheless, the data confirm the weak ϕ dependence of the collective diffusion coefficient of hard spheres, which reflects a strong cancellation between $H(0)$ and $S(0)$ in Eq. (7) and has also been observed in previous experiments [48,49].

VI. CONCLUSION

In this paper, experimental TCDLS data of the Q-dependent *short-time* diffusion coefficients $D_S(Q)$ for suspensions of slightly polydisperse PMMA particles have been compared to computational results obtained via a fluctuating LBE method. We have described an accurate method to obtain the experimental sample volume fraction ϕ by comparing the thermodynamic properties of our samples to those of a hard-sphere fluid. A precise determination of ϕ is necessary for an unambiguous comparison of the computational and experimental results. Good agreement was found between the two data sets at all particle volume fractions and for wave vectors Q ranging from the low Q limit to values of Q just beyond the first peak in the static structure factor $S(Q)$. This is a strong indication of both the validity of the sample volume fraction determination and the ability of the LBE method to simulate the complicated hydrodynamic interactions between the suspended particles. Comparisons of the short-time self-diffusion coefficient $D_S^S = D_S(Q \to \infty)$ have also been performed and good agreement is again obtained between the experimental and computational data. Moreover, for both the Q-dependent coefficients and the self-diffusion, we have compared our results to the theoretical predictions by Beenakker and Mazur and have confirmed the limits of validity of this theory. The small polydispersity of the experimental samples seems to have little effect on the measured dynamics.

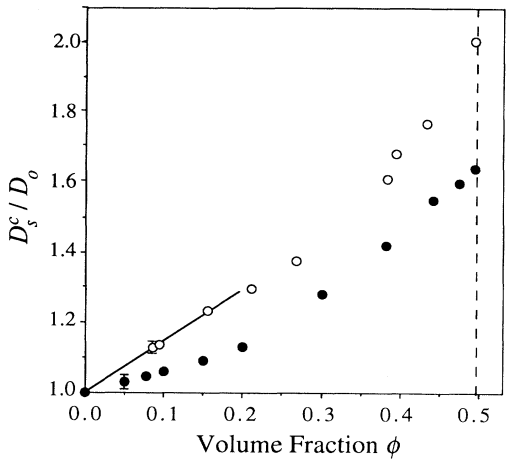

FIG. 9. Normalized short-time collective diffusion coefficients D_S^C/D_0. The closed symbols are the TCDLS results, the open symbols are the LBE results from purely dissipative measurements, and the solid line is the low-ϕ theory of Batchelor [47].

ACKNOWLEDGMENTS

O.P.B. gratefully acknowledges financial support from the Swiss Foundation for Scientific Research and Unilever Research, Port Sunlight, United Kingdom (UK). We thank S. M. Underwood for the gift of the PMMA particles, A. J C. Ladd for extremely useful discussions, and P. B. Warren and G. S. Pawley for advice and discussions. Livermore Computing at the Lawrence Livermore National Laboratory is gratefully acknowledged for generous amounts of computing time on the Meiko CS-2 and the EPSRC (UK) for time on the Cray T3D at the Edinburgh Parallel Computing Centre. We also thank D. J. Pine and B. J. Ackerson for making available to us a program for calculating the diffusion coefficients from the theory of Beenakker and Mazur.

[1] P. N. Pusey, in *Liquids, Freezing and the Glass Transition,* edited by J. P. Hansen, D. Levesque, and J. Zinn-Justin (Elsevier, Amsterdam, 1991), Chap. 10.
[2] C. W. J. Beenakker and P. Mazur, Physica A **126**, 349 (1984).
[3] M. Medina-Noyola, Phys. Rev. Lett. **60**, 2705 (1988).
[4] M. Tokuyama and I. Oppenheim, Phys. Rev. E **50**, R16 (1994).
[5] Y. Pomeau and P. Résibois, Phys. Lett. C **19**, 63 (1975), and references therein.
[6] B. J. Berne and R. Pecora, *Dynamic Light Scattering* (Wiley, New York, 1976).
[7] W. van Megen, R. H. Ottewill, S. M. Owens, and P. N. Pusey, J. Chem. Phys. **82**, 508 (1985).
[8] M. M. Kops-Werkhoven and H. M. Fijnaut, J. Chem. Phys. **74**, 1618 (1981).
[9] W. van Megen, S. M. Underwood, R. H. Ottewill, N. St. J. Wiliams, and P. N. Pusey, Faraday Discuss. Chem. Soc. **83**, 47 (1987); W. van Megen and S. M. Underwood, J. Chem. Phys. **91**, 552 (1989).
[10] D. J. Pine, D. A. Weitz, J. X. Zhu, and E. Herbolzheimer, J. Phys. (Paris) **51**, 2101 (1990).
[11] J. X. Zhu, D. J. Durian, J. Müller, D. A. Weitz, and D. J. Pine, Phys. Rev. Lett. **68**, 2559 (1992).
[12] L. Durlofsky, J. F. Brady, and G. Bossis, J. Fluid. Mech. **180**, 21 (1987).
[13] A. J C. Ladd, J. Chem. Phys. **93**, 3484 (1990).
[14] I. Snook, W. van Megen, and R. J. A. Tough, J. Chem. Phys. **78**, 5825 (1983).
[15] B. Cichocki and K. Hinsen, Physica A **166**, 473 (1990).
[16] K. Gaylor, I. Snook, and W. van Megen, J. Chem. Phys. **75**, 1682 (1981).
[17] W. van Megen and I. Snook, J. Chem. Soc., Faraday Trans. 2 **80**, 383 (1984).
[18] A. J. C. Ladd, Phys. Rev. Lett. **70**, 1339 (1993).
[19] A. J. C. Ladd, J. Fluid. Mech. **271**, 285 (1994); **271**, 311 (1994).
[20] O. P. Behrend, Phys. Rev. E **52**, 1164 (1995).
[21] A. J. C. Ladd, H. Gang, J. X. Zhu, and D. A. Weitz, Phys. Rev. Lett. **74**, 318 (1995).
[22] O. P. Behrend, P. N. Segrè, and P. N. Pusey (unpublished).
[23] P. N. Segrè, W. van Megen, P. N. Pusey, K. Schätzel, and W. Peters, J. Mod. Opt. **42**, 1929 (1995); M. Drewel, J. Ahrens, and U. Podschus, J. Opt. Soc. Am. **7**, 206 (1990).
[24] J.-P. Hansen and I. R. McDonald, *Theory of Simple Liquids* (Academic, London, 1986).
[25] L. Verlet and J. J. Weis, Phys. Rev. A **5**, 939 (1972).
[26] L. Antl, J. W. Goodwin, R. D. Hill, R. H. Ottewill, S. M. Owens, S. Papworth, and J. W. Waters, Colloids Surf. **17**, 67 (1986).
[27] D. E. Koppel, J. Chem. Phys. **57**, 4814 (1972); J. C. Brown, P. N. Pusey, and R. Deitz, *ibid.* **62**, 1136 (1975).
[28] P. N. Pusey and W. van Megen, Nature **320**, 340 (1986); S. M. Underwood, J. R. Taylor, and W. van Megen, Langmuir **10**, 3550 (1994).
[29] W. G. Hoover and F. H. Ree, J. Chem. Phys. **49**, 3609 (1968).
[30] S. E. Paulin and B. J. Ackerson, Phys. Rev. Lett. **64**, 2663 (1990).
[31] P. N. Pusey and W. van Megen, J. Chem. Phys. **80**, 3513 (1984).
[32] D. Frenkel, R. J. Vos, C. G. de Kruif, and A. Vrij, J. Chem. Phys. **84**, 4625 (1986); P. van Beurten and A. Vrij, *ibid.* **74**, 2744 (1981).
[33] U. Frisch, D. d'Humières, B. Hasslacher, P. Lallemand, Y. Pomeau, and J.-P. Rivet, Complex Syst. **1**, 649 (1987).
[34] R. Benzi, S. Succi, and M. Vergassola, Phys. Rep. **222**, 147 (1992).
[35] S. Chapman and T. G. Cowling, *The Mathematical Theory of Non-Uniform Gases,* 2nd ed. (Cambridge University Press, Cambridge, 1952).
[36] Y. H. Qian, D. d'Humières, and P. Lallemand, Europhys. Lett. **17**, 479 (1992).
[37] S. Chen, Z. Wang, X. Shan, and G. D. Doolen, J. Stat. Phys. **68**, 379 (1992).
[38] L. D. Landau and E. M. Lifshitz, *Fluid Mechanics* (Pergamon, Oxford, 1959).
[39] H. Hasimoto, J. Fluid. Mech. **5**, 317 (1959).
[40] R. J. Phillips and J. F. Brady, Phys. Fluids **31**, 3462 (1988).
[41] D. Bedeaux, J. Colloid Interface Sci. **118**, 80 (1987).
[42] J. C. van der Werff, C. G. de Kruif, C. Blom, and J. Mellema, Phys. Rev. A **39**, 795 (1989).
[43] W. van Megen and S. M. Underwood, Phys. Rev. E **42**, 4206 (1994).
[44] L. V. Woodcock and C. A. Angell, Phys. Rev. Lett. **47**, 1129 (1981).
[45] P. N. Pusey and W. van Megen, J. Phys. (Paris) **44**, 285 (1983).
[46] P. N. Pusey, J. Phys. A **11**, 119 (1978); R. Krause, J. L. Arauz-Lara, G. Nägele, H. Ruiz-Estrada, M. Medina-Noyola, R. Weber, and R. Klein, Physica A **178**, 241 (1991).
[47] G. K. Batchelor, J. Fluid. Mech. **52**, 245 (1972); **74**, 1 (1976).
[48] M. M. Kops-Werkhoven and H. M. Fijnaut, J. Chem. Phys. **77**, 2242 (1982).
[49] D. J. Cebula, R. H. Ottewill, J. Ralston, and P. N. Pusey, J. Chem. Soc. Faraday Trans. 1 **77**, 2585 (1981).